

Article

Synthesis, Molecular Docking, Molecular Dynamics Studies, and In Vitro Biological Evaluation of New Biofunctional Ketoprofen Derivatives with Different N-Containing Heterocycles

Stanimir Manolov ¹, Dimitar Bojilov ¹, Iliyan Ivanov ^{1,*}, Gabriel Marc ², Nadezhda Bataklieva ¹, Smaranda Oniga ³, Ovidiu Oniga ² and Paraskev Nedialkov ⁴

¹ Department of Organic Chemistry, Faculty of Chemistry, University of Plovdiv, 24 "Tsar Assen" Street, 4000 Plovdiv, Bulgaria; manolov@uni-plovdiv.net (S.M.); bozhilov@uni-plovdiv.net (D.B.); nadi_d@abv.bg (N.B.)

² Department of Pharmaceutical Chemistry, Faculty of Pharmacy, "Iuliu Hațieganu" University of Medicine and Pharmacy, 41 Victor Babeș Street, 400010 Cluj-Napoca, Romania; marc.gabriel@umfcluj.ro (G.M.); ooniga@umfcluj.ro (O.O.)

³ Department of Therapeutic Chemistry, "Iuliu Hațieganu" University of Medicine and Pharmacy, 12 Ion Creangă Street, 400010 Cluj-Napoca, Romania; smaranda.oniga@umfcluj.ro

⁴ Department of Pharmacognosy, Faculty of Pharmacy, Medical University of Sofia, 2 Dunav Street, 1000 Sofia, Bulgaria; pnedialkov@pharmfac.mu-sofia.bg

* Correspondence: iiliyan@abv.bg; Tel./Fax: +359-32-261-349



Citation: Manolov, S.; Bojilov, D.; Ivanov, I.; Marc, G.; Bataklieva, N.; Oniga, S.; Oniga, O.; Nedialkov, P. Synthesis, Molecular Docking, Molecular Dynamics Studies, and In Vitro Biological Evaluation of New Biofunctional Ketoprofen Derivatives with Different N-Containing Heterocycles. *Processes* **2023**, *11*, 1837. <https://doi.org/10.3390/pr11061837>

Academic Editors:
Alexander Novikov and
Andrea Temperini

Received: 25 May 2023
Revised: 15 June 2023
Accepted: 15 June 2023
Published: 17 June 2023



Copyright: © 2023 by the authors. Licensee MDPI, Basel, Switzerland. This article is an open access article distributed under the terms and conditions of the Creative Commons Attribution (CC BY) license (<https://creativecommons.org/licenses/by/4.0/>).

Abstract: Herein, we report the synthesis of four new hybrid molecules between ketoprofen or 2-(3-benzoylphenyl)propanoic acid and N-containing heterocyclic compounds, such as piperidine, pyrrolidine, 1,2,3,4-tetrahydroquinoline, and 1,2,3,4-tetrahydroisoquinoline. The obtained hybrid compounds were fully characterized using ¹H- and ¹³C-NMR, UV-Vis, and HRMS spectra. Detailed HRMS analysis is provided for all novel hybrid molecules. The compounds were assessed for their *in vitro* anti-inflammatory and antioxidant activity. The lipophilicity of the hybrids was determined, both theoretically (*cLogP*) and experimentally (*R_M*). The affinity of the compounds to the human serum albumin was assessed *in silico* by molecular docking study using two software, and the stability of the predicted complexes was evaluated by molecular dynamics study. All novel hybrids have shown very good *HPSA* activity, statistically close when compared to the reference—quercetin. The molecular docking confirmed the obtained *in vitro* results. Tetrahydroquinoline derivative **3c** and tetrahydroisoquinoline derivative **3d** have the highest affinity for albumin. They show stronger anti-inflammatory action than their predecessor, ketoprofen and the regularly used ibuprofen.

Keywords: ketoprofen; pyrrolidine; piperidine; 1,2,3,4-tetrahydroquinoline; 1,2,3,4-tetrahydroisoquinoline; hybrid molecules; *in vitro* biological activity; molecular docking; molecular dynamics

1. Introduction

N-heterocycles can be found in natural products and drug molecules and are indispensable components in the fields of organic synthesis, medicinal chemistry and materials science. The construction of these N-containing heterocycles by traditional methods usually requires the preparation of reactive intermediates. Through in recent decades, with the rapid advent of transition metal-catalyzed reactions, the synthesis of heterocycles from precursors with inert chemical bonds has become a challenge. Many have developed efficient methods for the preparation of N-heterocyclic compounds, such as aziridines, azetidines, indoles and quinolines and many others [1].

Pyrrolidine **1a** (Figure 1), also known as tetrahydropyrrole, is an organic compound with molecular formula (CH₂)₄NH. It is a cyclic secondary amine, also classified as a

saturated heterocycle. Many modifications of pyrrolidine are found in natural and synthetic drugs and drug candidates [2].

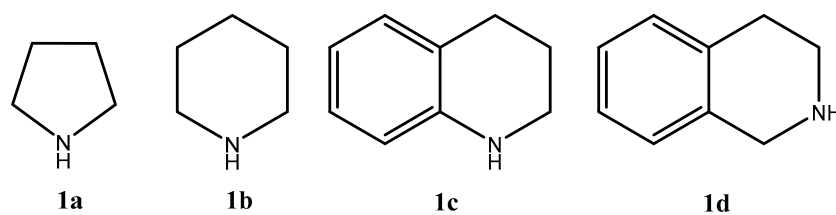


Figure 1. Structural formulas of pyrrolidine **1a**, piperidine **1b**, 1,2,3,4-tetrahydroquinoline **1c**, and 1,2,3,4-tetrahydroisoquinoline **1d**.

The pyrrolidine ring structure (Figure 1) is present in many natural alkaloids, such as nicotine and hygrin [3]. It is found in many medicines, such as procyclidine and bepridil. It also forms the basis for racetam compounds (e.g., piracetam and aniracetam). The amino acids proline and hydroxyproline are structurally derived from pyrrolidine [2]. Pyrrolidine is widely found in the literature as a fragment—part of a number of organic compounds possessing a number of biological activities, such as antiviral, anti-inflammatory, antibacterial, antidepressant, etc. [4].

Piperidine **1b** (Figure 1) is a key heterocyclic amine that is part of a number of pharmaceutical products and natural alkaloids, possessing a diverse range of biological activities [5]. Piperidine fragment **1b** is present in a vast array of natural alkaloids and approved pharmaceuticals [6]. For example, the alkaloid piperine gives a spicy taste in black pepper [7]. This six-membered nitrogen-containing fully saturated ring is also found in stimulants (methylphenidate, pipradrol etc.), vasodilators (minoxidil), antipsychotics (droperidol, melperone, etc.), opioids (pethidine, fentanyl, etc.) and many others drugs.

The fully hydrogenated quinoline or 1,2,3,4-tetrahydroquinoline **1c** (Figure 1) is another example of a nitrogen-containing fragment that is widely distributed in nature and the same in pharmaceuticals. The structure of 1,2,3,4-tetrahydroquinoline **1c** is a very common structural motif and is found in numerous biologically active natural products and pharmacologically relevant therapeutic agents [8].

1,2,3,4-tetrahydroisoquinoline **1d** (Figure 1) is another cyclic secondary amine, widely distributed in nature, forming the isoquinoline alkaloids family. Many synthetic and natural molecules containing 1,2,3,4-tetrahydroisoquinoline skeleton have been reported to possess a wide range of pharmacological activities like antibacterial, anti-inflammatory, antifungal, antiviral, antimalarial, and anticancer, among others [9–14].

First synthesized back in 1967, ketoprofen continues to be widely used, and its interest continues to this day. It belongs to the group of nonsteroidal anti-inflammatory drugs (NSAIDs) belonging to the family of propionic derivatives of arylpropionic acid [15].

Ketoprofen (Figure 2) widespread use is mainly due to its antipyretic, analgesic and anti-inflammatory properties due to reversible inhibition of cyclooxygenase 1 and 2 (COX-1 and COX-2), which in turn reduces the production of pro-inflammatory prostaglandin precursors [16].

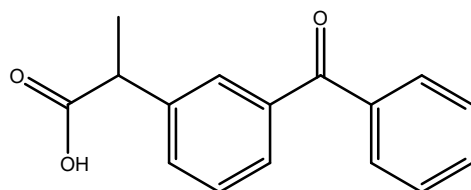


Figure 2. The structural formula of ketoprofen.

Because of the importance of these scaffolds in drug discovery and pharmaceutical chemistry, the development of new methodologies for the synthesis of new hybrids of

N-containing heterocyclic derivatives remains to be a very active field of research, as evidenced by the publication of more than 500 articles in the field in recent years.

Obtaining new hybrid molecules constructed from ketoprofen fragments attached to an *N*-containing heterocycle is particularly fascinating in order to examine its bio functionality.

2. Materials and Methods

2.1. General

The reagents were purchased from commercial suppliers (Sigma-Aldrich S.A. and Riedel-de Haën, Sofia, Bulgaria) and used as received. A Bruker NEO 400 (400/100 MHz $^1\text{H}/^{13}\text{C}$) spectrometer was used for the recording of the NMR spectral data (BAS-IOCCP—Sofia, Bruker, Billerica, MA, USA). All compounds were analyzed in CDCl_3 at 400 MHz and 101 MHz for ^1H -NMR and ^{13}C -NMR, respectively. Chemical shifts were determined to tetramethylsilane (TMS) ($\delta = 0.00$ ppm) as an internal standard; the coupling constants are given in Hz. Recorded NMR spectra were taken at room temperature (approx. 295 K). Absorbance was measured with a spectrophotometer Camspec M508, Leeds, UK. The high-resolution mass (HRMS) analysis was carried out on a Q Exactive Plus mass spectrometer with a heated electrospray ionization source (HESI-II) (Thermo Fisher Scientific, Inc., Bremen, Germany) coupled with an ultrahigh-performance liquid chromatography (UHPLC) system Dionex Ultimate 3000RSLC (Thermo Fisher Scientific, Inc.) consisting of 6-channel degasser SRD-3600, high-pressure gradient pump HPG-3400RS, autosampler WPS-3000TRS, column compartment TCC-3000RS, and narrow bore Hypersil GOLDTM C18 (2.1 \times 50 mm, 1.9 μm) column. For the TLC analysis, precoated 0.2 mm Fluka silica gel 60 plates (Merck KGaA, Darmstadt, Germany) were used.

2.2. Synthesis

2.2.1. Synthesis of 2-(3-benzoylphenyl)propanoyl chloride **2**

To ketoprofen (1 mmol, 0.254 g) dissolved in toluene (30 mL), an excess of thionyl chloride (1.2 mmol, 0.087 mL) was added. The reaction mixture was stirred under reflux for two hours. The excess of thionyl chloride and the toluene were removed under reduced pressure. The obtained 2-(3-benzoylphenyl)propanoyl chloride **2** was used without further purification.

2.2.2. Synthesis of Compounds **3a–d**

To a solution of corresponding amines **1a–d** (1 mmol) in dichloromethane (30 mL), an equal amount of 2-(3-benzoylphenyl)propanoyl chloride **2** (1 mmol, 0.272 g) was added. After 10 min, triethylamine (1.2 mmol, 0.121 g) was added to the solution. After 30 min, the solution was washed with diluted hydrochloric acid, saturated solution of Na_2CO_3 , and brine. The combined organic layers were dried over anhydrous Na_2SO_4 , and the solvent was removed under reduced pressure. The new hybrid molecules were purified by filtration through short-column chromatography over neutral Al_2O_3 .

3a 2-(3-benzoylphenyl)-1-(pyrrolidin-1-yl)propan-1-one.

Light-yellow oil, Yield: 97% (0.299 g), $R_f = 0.45$ (diethyl ether), ^1H NMR (400 MHz, CDCl_3) δ 7.74–7.69 (m, 2H), 7.65 (t, $J = 1.8$ Hz, 1H), 7.57 (ddd, $J = 7.6, 1.7, 1.2$ Hz, 1H), 7.54–7.48 (m, 2H), 7.43–7.33 (m, 3H), 3.76 (q, $J = 6.9$ Hz, 1H), 3.50–3.38 (m, 2H), 3.38–3.11 (m, 2H), 1.87–1.76 (m, 2H), 1.75–1.69 (m, 2H), 1.42 (d, $J = 6.9$ Hz, 3H). ^{13}C NMR (101 MHz, CDCl_3) δ 196.63 (Ph-CO-Ph), 171.72 (C=O), 142.09 (Ar), 137.92 (Ar), 137.53 (Ar), 132.54 (Ar), 131.49 (Ar), 130.08 (Ar), 129.26 (Ar), 129.03 (Ar), 128.75 (Ar), 128.30 (Ar), 46.41 (CH₂-N), 46.11 (CH₂-N), 44.73 (CH), 26.10 (CH₂), 24.17 (CH₂), 20.12 (CH₃). UV λ_{max} , MeOH: 276 ($\epsilon = 15,270$) nm. HRMS Electrospray ionization (ESI) m/z calcd for $[\text{M}+\text{H}]^+$ $\text{C}_{20}\text{H}_{22}\text{NO}_2^+$ = 308.1645, found 308.1638 (mass error $\Delta m = -2.27$ ppm), calcd for $[\text{M}+\text{Na}]^+$ $\text{C}_{20}\text{H}_{21}\text{NO}_2\text{Na}^+$ = 330.1465, found 330.1458 (mass error $\Delta m = -2.12$ ppm).

3b 2-(3-benzoylphenyl)-1-(piperidin-1-yl)propan-1-one.

Light yellow oil, Yield: 94% (0.302 g), $R_f = 0.85$ (diethyl ether), ^1H NMR (400 MHz, CDCl_3) δ 7.73–7.69 (m, 2H), 7.62 (t, $J = 1.8$ Hz, 1H), 7.56 (dt, $J = 7.6, 1.4$ Hz, 1H), 7.54–7.49

(m, 1H), 7.46 (dt, $J = 7.9, 1.5$ Hz, 1H), 7.41 (dd, $J = 8.2, 6.9$ Hz, 2H), 7.36 (t, $J = 7.6$ Hz, 1H), 3.91 (q, $J = 6.9$ Hz, 1H), 3.50 (dddd, $J = 105.8, 12.9, 6.5, 3.1$ Hz, 2H), 3.27 (t, $J = 5.5$ Hz, 2H), 1.53–1.44 (m, 3H), 1.40 (d, $J = 6.8$ Hz, 3H), 1.33 (dtd, $J = 17.1, 7.6, 4.6$ Hz, 2H), 1.01 (dp, $J = 12.1, 5.8$ Hz, 1H). ^{13}C NMR (101 MHz, CDCl_3) δ 196.59 (Ph-CO-Ph), 171.26 (C=O), 142.74 (Ar), 138.08 (Ar), 137.54 (Ar), 132.54 (Ar), 131.23 (Ar), 130.05 (Ar), 128.96 (Ar), 128.79 (Ar), 128.59 (Ar), 128.31 (Ar), 46.65 ($\text{CH}_2\text{-N}$), 43.19 ($\text{CH}_2\text{-N}$), 42.82 (CH), 26.13 ($\text{CH}_2\text{-CH}_2\text{-CH}_2$), 25.52 ($\text{CH}_2\text{-CH}_2\text{-CH}_2$), 24.49 ($\text{CH}_2\text{-CH}_2\text{-CH}_2$), 20.64 (CH_3). UV λ_{max} , MeOH: 276 ($\epsilon = 18,500$) nm. HRMS Electrospray ionization (ESI) m/z calcd for $[\text{M}+\text{H}]^+ \text{C}_{21}\text{H}_{24}\text{NO}_2^+ = 322.1802$, found 322.1795 (mass error $\Delta m = -2.17$ ppm), calcd for $[\text{M}+\text{Na}]^+ \text{C}_{21}\text{H}_{23}\text{NO}_2\text{Na}^+ = 344.1621$, found 344.1614 (mass error $\Delta m = -2.03$ ppm).

3c 2-(3-benzoylphenyl)-1-(3,4-dihydroquinolin-1(2H)-yl)propan-1-one.

Light-yellow oil, Yield: 95% (0.352 g), $R_f = 0.48$ (petroleum/diethyl ether = 1/1), ^1H NMR (400 MHz, CDCl_3) δ 7.70–7.62 (m, 2H), 7.57–7.47 (m, 2H), 7.43–7.31 (m, 4H), 7.28 (t, $J = 7.5$ Hz, 1H), 7.16–6.90 (m, 4H), 4.33–4.21 (m, 1H), 3.85 (s, 1H), 3.50 (dt, $J = 13.0, 6.7$ Hz, 1H), 2.54–2.41 (m, 1H), 2.23 (s, 1H), 1.81 (dp, $J = 13.2, 6.6$ Hz, 1H), 1.71 (s, 1H), 1.44 (d, $J = 6.9$ Hz, 3H). ^{13}C NMR (101 MHz, CDCl_3) δ 196.61 (Ph-CO-Ph), 171.52 (C=O), 142.17 (Ar), 137.87 (Ar), 137.66 (Ar), 132.59 (Ar), 131.42 (Ar), 130.15 (Ar), 129.34 (Ar), 128.68 (Ar), 128.57 (Ar), 128.42 (Ar), 126.30 (Ar), 125.09 (Ar), 42.90 (CH), 26.38 (CH_2), 24.12 (CH_2), 20.29 (CH_3). UV λ_{max} , MeOH: 273 ($\epsilon = 6940$) nm. HRMS Electrospray ionization (ESI) m/z calcd for $[\text{M}+\text{H}]^+ \text{C}_{25}\text{H}_{24}\text{NO}_2^+ = 370.1802$, found 370.1795 (mass error $\Delta m = -1.89$ ppm), calcd for $[\text{M}+\text{Na}]^+ \text{C}_{25}\text{H}_{23}\text{NO}_2\text{Na}^+ = 392.1621$, found 392.1613 (mass error $\Delta m = -2.04$ ppm).

3d 2-(3-benzoylphenyl)-1-(3,4-dihydroisoquinolin-2(1H)-yl)propan-1-one.

Light-yellow oil, Yield: 95% (0.350 g), $R_f = 0.59$ (diethyl ether), ^1H NMR (400 MHz, CDCl_3) δ 7.70–7.61 (m, 3H), 7.59–7.44 (m, 3H), 7.41–7.30 (m, 3H), 7.12–7.01 (m, 3H), 7.00–6.79 (m, 1H), 4.79–4.60 (m, 1H), 4.60–4.33 (m, 1H), 4.05–3.72 (m, 2H), 3.62–3.49 (m, 1H), 2.79–2.31 (m, 2H), 1.43 (dd, $J = 6.9, 3.0$ Hz, 3H). ^{13}C NMR (101 MHz, CDCl_3) δ 196.52 (Ph-CO-Ph), 172.09 (C=O), 142.32 (Ar), 138.17 (Ar), 137.43 (Ar), 133.92 (Ar), 133.41 (Ar), 132.58 (Ar), 131.27 (Ar), 131.25 (Ar), 130.04 (Ar), 129.00 (Ar), 128.90 (Ar), 128.77 (Ar), 128.31 (Ar), 126.69 (Ar), 126.55 (Ar), 126.28 (Ar), 47.39 (CH_2), 44.70 (CH_2), 43.39 (CH), 29.19 (CH_2), 20.65 (CH_3). UV λ_{max} , MeOH: 235 ($\epsilon = 16,100$) nm, 276 ($\epsilon = 10,400$) nm. HRMS Electrospray ionization (ESI) m/z calcd for $[\text{M}+\text{H}]^+ \text{C}_{25}\text{H}_{24}\text{NO}_2^+ = 370.1802$, found 370.1795 (mass error $\Delta m = -1.89$ ppm), calcd for $[\text{M}+\text{Na}]^+ \text{C}_{25}\text{H}_{23}\text{NO}_2\text{Na}^+ = 392.1621$, found 392.1613 (mass error $\Delta m = -2.04$ ppm).

2.3. HRMS Analysis

Operating conditions for the HESI source used in a positive ionization mode were: +3.5 kV spray voltage, 320 °C capillary and probe heater temperature, sheath gas flow rate 36 a.u., auxiliary gas flow rate 11 a.u., spare gas flow rate 1 a.u. (a.u. refer to arbitrary values set by the Exactive Tune software) and S-Lens RF level 50.00. Nitrogen was used for sample nebulization and collision gas in the HCD cell. The aliquots of 1 μL of the solutions of the samples (ca. 20 $\mu\text{g mL}^{-1}$) were introduced into the mass spectrometer through the UHPLC system. Each chromatographic run was carried out isocratically with a mobile phase consisting of water-acetonitrile-methanol-acetic acid (25:50:25:0.2). The solvent flow rate was 300 $\mu\text{L min}^{-1}$. Full MS—ddMS² (Top5) was used as an MS experiment, where in full scan MS, the resolution, automatic gain control (AGC) target, maximum injection time (IT), and mass range were 70,000 (at m/z 200), 3×10^6 , 100 ms, and m/z 100–500, respectively. The instrument parameters for ddMS² scans were as follows: the resolution was 17,500 (at m/z 200), AGC target was 1×10^5 , maximum IT was 50 ms, loop count was 5, isolation window 2.0 m/z , stepped normalized collision energy (NCE) was set to 10, 20, 60. The data-dependent (dd) settings were as follows: maximum ACG target was 5×10^4 , dynamic exclusion was set to 1 s, preferred peptide match and switched on isotope exclusion were used. Xcalibur (Thermo Fisher Scientific, Waltham, MA, USA) ver. 4.0 was used for data acquisition and processing.

2.4. In Vitro Analysis

2.4.1. Hydrogen Peroxide Scavenging Activity (HPSA)

The Manolov et al. method was used to assess the hydrogen peroxide scavenging capability [17]. A 43 mM solution of H₂O₂ was prepared in a potassium phosphate buffer solution (0.2 M, pH 7.4). The analysis of the samples was carried out as follows: in test tubes, 0.6 mL H₂O₂ (43 mM), 1 mL sample/standard with different concentrations (20–1000 µg/mL), and 2.4 mL potassium phosphate buffer solution were mixed. The mixture was stirred and incubated in the dark for 10 min at 37 °C. Absorbance was measured at 230 nm with a spectrophotometer (Camspec M508, Leeds, UK) against a blank solution containing phosphate buffer and H₂O₂ without the sample. Ascorbic acid and quercetin were used as standards. The percentage HPSA of the samples was evaluated by comparing it with a blank sample and calculated using the following formula:

$$I, \%(HPSA) = \left[\frac{A_{blank} - (A_{TS} - A_{CS})}{A_{blank}} \right] \times 100$$

where A_{blank} is the absorbance of the blank sample, A_{CS} is the absorbance of the control sample, and A_{TS} is the absorbance of the test sample.

2.4.2. Inhibition of Albumin Denaturation (IAD)

In vitro, analysis of anti-inflammatory activity was assessed as inhibition of albumin denaturation (IAD). The analysis was performed according to Manolov et al. method [18] with minor modifications. The experiment was performed with human albumin. The solution of albumin (1%) was prepared in distilled water (pH 7.4). The tested compounds/standard were dissolved firstly in PBS, so the final concentration of the stock solution was 1000 µg/mL. Then a series of working solutions with different concentrations (20–500 µg/mL) in PBS were prepared. The reaction mixture was containing 2 mL test sample/standard of different concentrations and 1 mL albumin (1%). The mixture was incubated at 37 °C for 15 min and then heated at 70 °C for 15 min in a water bath. After cooling, the turbidity was measured at 660 nm with a spectrophotometer (Camspec M508, Leeds, UK). Ibuprofen and ketoprofen were used as standards. The experiment was performed three times. Percentage inhibition of albumin denaturation (IAD) was calculated against the control. The control sample is albumin with the same concentration dissolved in distilled water.

$$\%IAD = \left[\frac{A_{blank} - A_{sample}}{A_{blank}} \right] \times 100$$

2.4.3. Determination of Lipophilicity as cLogP

The lipophilicity of the compounds was calculated using the software: ACD/ChemSketch/LogP Predictor v.14.08.

2.4.4. Molecular Docking

The molecular docking of the ligands was performed using AutoDock Vina 1.1.2 (ADV) and AutoDock 4.2 (AD) [19,20] against the human serum albumin (HSA), deposited with the entry code 7JWN in the Protein Data Bank [21]. Two software were chosen for molecular docking because although their names are similar, the principle on which they work is different. Because it is known that molecular docking studies may generate false positive results, the use of two software that works differently can be used for cross-validation of the results [22]. Supplementary, AD possesses an intrinsic tool that performs a rapid clustering analysis to confirm that the best binding pose is one of the most found poses from the total of poses generated.

For each compound, two ligand files were created, one for each R and S isomer using Avogadro 1.2.0 and following the previously reported protocol [23,24].

The preparation of the macromolecule as the target was performed according to the standard procedure previously reported by our group—removal of the co-crystallized molecules, addition of the polar hydrogen atoms and addition of charges [25].

The final preparation of the files of ligands and macromolecules was performed using AutoDockTools 1.5.6 [20].

Four main potential binding sites were targeted in the molecular docking study—Sudlow site I (subdomain IIA), Sudlow II (subdomain IIIA), site III and cleft. The reason for this choice is that, to the best of our knowledge, the other binding sites reported in the literature have a limited role in drug binding, and the sites we have chosen are the most important in drug binding to albumin [26–31].

The search space for each potential binding site was set as a cube, with sides equal to 20 for ADV and 54 for AD (spacing = 0.375). The cartesian coordinates of the center of the search space for each site were set as follows: for site Sudlow 1 $x = 30.62$, $y = 25.50$, $z = 12.43$, for site Sudlow 2 $x = 5.95$, $y = 18.22$, $z = 21.06$, for site 3 $x = 30.15$, $y = 26.98$, $z = 37.99$ and for cleft site $x = 20.89$, $y = 21.74$, $z = 22.43$.

In order to obtain results with higher reproducibility, ADV was requested to generate 20 poses for each ligand in each binding site, while AD was requested to generate 200 poses in order to perform the cluster analysis in the limit of 2 Å root mean square deviation of the coordinates of atoms.

The visualization of the results of the molecular docking study was performed using Chimera 1.10.2 [32].

2.4.5. Molecular Dynamics

To evaluate the stability in a time of the ligand–albumin complexes, some molecular dynamics simulations were performed with GROMACS 2023 [33] using the CHARMM36 force field [34] on a machine running Debian 11. The computer has an Intel Core 7700 K CPU and an NVIDIA RTX 3060 GPU. Their interoperability was based on CUDA 12. Ligands parametrization was made using the CgenFF server [34].

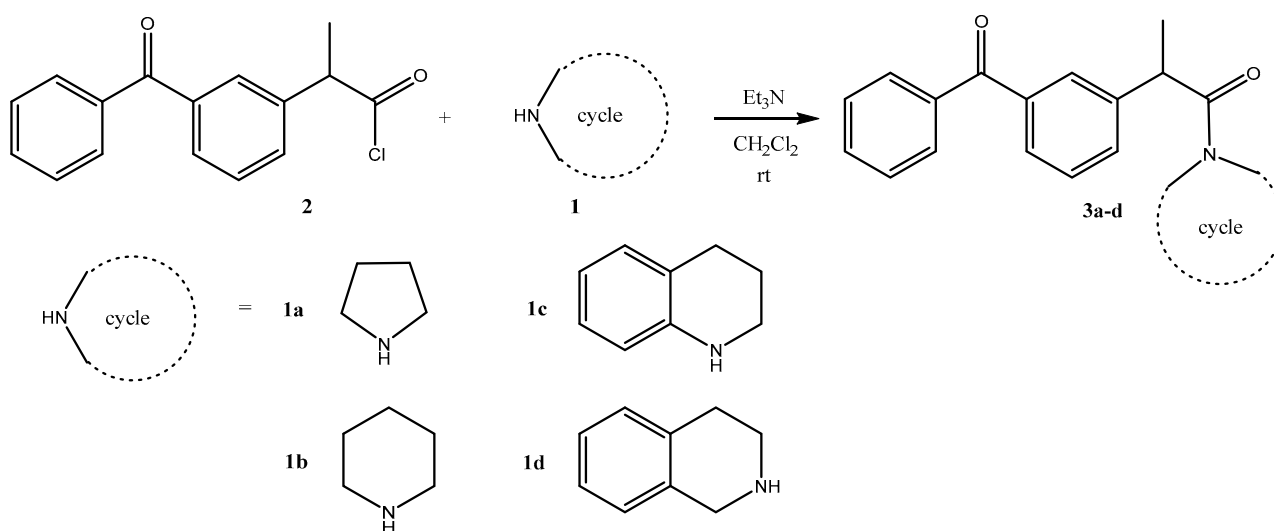
The protein and the ligands were placed in an orthorhombic box with a 1 nm gap at the sides and were filled using the TIP3P solvation water model [35]. The preparation of the systems and running of the simulations were made according to the previous works reported [36–38]. Briefly, the main parameters used for carrying out molecular dynamics studies will be presented. The constructed systems were neutralized by adding sodium ions. The energy of the systems was minimized for 5000 steps using the steepest descent method, and the convergence was reached until the maximum force $<1000 \text{ KJ mol}^{-1} \cdot \text{nm}^{-1}$ to remove the steric clashes. The equilibration of the systems was made at NVT and NPT ensembles at 300 K for 100 ps (50,000 steps \times 2 fs) each. The production of the simulations was run for 100 ns (50,000,000 \times 2 fs) at 300 K and 1 bar with periodic boundary conditions on all axes.

Visualization of the evolution in time of the ligand–albumin complexes during the molecular dynamics simulation was made using VMD 1.9.4 [39].

3. Results and Discussion

3.1. Synthesis

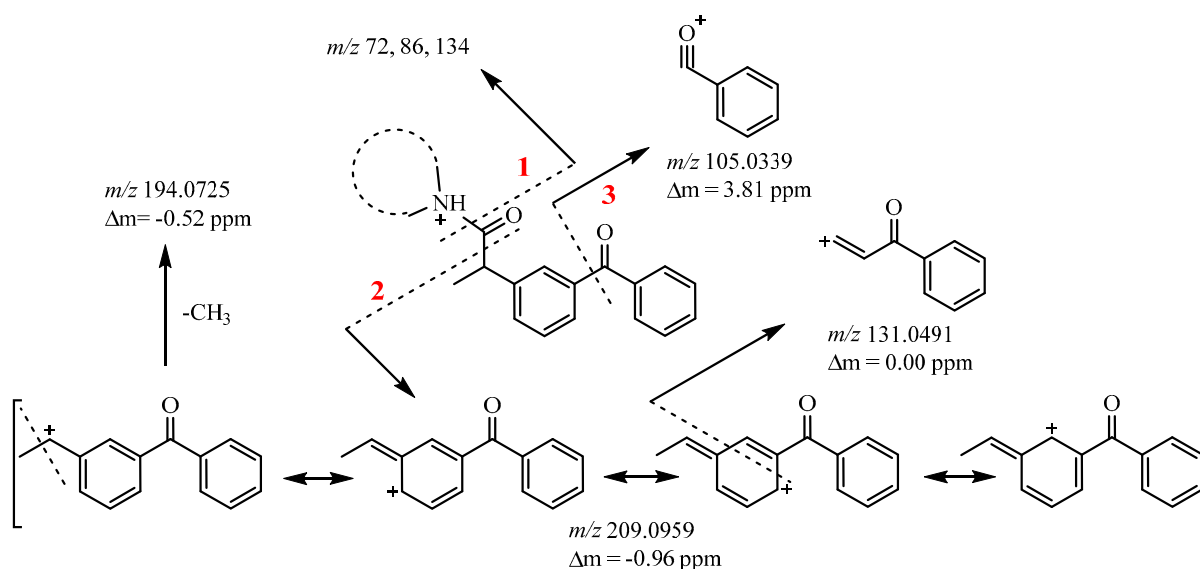
In this article, we report the successful synthesis of four ketoprofen hybrid molecules with different *N*-containing compounds, such as pyrrolidine **1a**, piperidine **1b**, 1,2,3,4-tetrahydroquinoline **1c**, and 1,2,3,4-tetrahydroisoquinoline **1d** (Figure 1), as shown in Scheme 1. In Scheme 1, we report the synthesis of four novel ketoprofen hybrid compounds. Ning and co-workers report the synthesis and characterization of the fluorinated product of compound **3a** [40]. The second reported by us, molecule **3b**, partially consists of the molecule reported by a group of Turkish scientists [41]. There was no information available in chemical databases for compounds **3c** and **3d**.



Scheme 1. Synthesis of hybrids **3a–d**.

3.2. Mass Analysis

Compounds **3a–d** have a common pharmacophore—ketoprofen. The only difference in these compounds is in the *N*-containing heterocyclic rings—pyrrolidine, piperidine, benzo[*b*]piperidine, and benzo[*c*]piperidine. We used mass spectrometry to probe their structure. The heterocyclic rings and ketoprofen are linked by a common structural fragment *N*-C(=O)-C. Under MS/MS conditions, three pathways of molecular ion fragmentation were established. The main fragmentation pathways of compounds **3a–d** include the cleavage of the *N*-C (path 1), C-C (path 2) bonds and the cleavage of the structural fragment C-C(=O)-C (path 3) connecting the two aromatic cores (Scheme 2).



Scheme 2. General fragmentation scheme of ketoprofen derivatives **3a–d**.

Cleavage of the *N*-C bond (path 1) provides important information about the structure of the heterocyclic ring (m/z 72, 86, 134) (Scheme 2, Figures S14, S16, S18 and S20). Cleavage of the C-C bond (path 2) leads to a resonance-stable aromatic cation (m/z 209) characteristic of ketoprofen, established in our previous studies (Scheme 2) [42]. Under ESI-MS conditions, the same ion undergoes loss of the CH_3 radical to yield an ion with m/z 194. Furthermore, the fragment ion with m/z 131 results from the retrocyclization of the resonance cation m/z 209 (Scheme 2). Fragmentation carried out in route 3 gave an m/z 105 ion resulting from

cleavage of the diphenyl ketone fragment (Scheme 2). Compounds **3c** and **3d** are isomers and have ion m/z 370 (Figures S17 and S19). In the fragmentation between the two isomers, a significant difference is observed, which is mainly expressed in the splitting of ion m/z 134 (Figures S18 and S20).

It is the product ion of both isomers, i.e., it corresponds to benzo[*b*]piperidine (1,2,3,4 tetrahydroquinoline nucleus) and benzo[*c*]piperidine (1,2,3,4 tetrahydroisoquinoline nucleus). In the MS/MS experiment, only benzo[*c*]piperidine was found to fragment to the characteristic ion with m/z 117 (Figure S20) [43]. Furthermore, a difference in the m/z 209 and m/z 105 ion intensities was observed in favor of benzo[*b*]piperidine, with the ratio between the two intensities being 2.17 and 1.45 for 209 and 105, respectively (Figures S18 and S20).

3.3. In Vitro Biological Assessment

All synthesized ketoprofen hybrids were tested for their *in vitro* inhibition of albumin denaturation (*IAD*) and hydrogen peroxide scavenging activity (*HPSA*). The obtained *in vitro* results are compared with the *in silico* predictions. The results of the study are presented in Table 1.

Table 1. *In vitro* results of the conducted biological activity.

Compounds	HPSA	IAD	$R_M \pm SD$	cLogP
	IC ₅₀ , µg/mL			
Ascorbic acid	24.84 ± 0.35	-	-	-
Quercetin	69.25 ± 1.82	-	-	-
Ibuprofen	-	81.50 ± 4.95	1.11 ± 0.010	3.72
Ketoprofen	-	126.58 ± 5.00	1.64 ± 0.006	3.59
3a	85.09 ± 0.24	167.02 ± 8.05	2.07 ± 0.010	4.10
3b	69.98 ± 0.50	130.28 ± 0.41	1.92 ± 0.005	4.61
3c	71.44 ± 0.27	77.18 ± 1.08	1.95 ± 0.008	5.91
3d	59.47 ± 0.36	73.59 ± 1.67	2.25 ± 0.010	5.09

3.3.1. Hydrogen Peroxide Scavenging Activity (*HPSA*)

Reactive oxygen species (ROS) are chemically reactive oxygen radicals and molecules [superoxide ($O_2^{\bullet-}$), hydroxyl ($\bullet OH$), peroxy ($ROO\bullet$) and alkoxy ($RO\bullet$), HOCl, ozone (O_3), peroxyxynitrite ($ONOO^-$), singlet oxygen (1O_2), and H_2O_2]. They are generated as a natural consequence of biological metabolism. Enzyme systems control ROS levels under physiological circumstances. They have been shown to cause harm to critical biological substances, such as phospholipids, proteins, and DNA. It has been established that the harm they inflict contributes to the development of a variety of illnesses (cancer, cardiovascular disease, atherosclerosis, and Alzheimer's disease) [44]. Even in a condition of physiological health, the harmful consequences of accumulating oxygen and its derivatives in the body contribute to a reduction in life expectancy [45].

The results for hydrogen peroxide scavenging activity (*HPSA*) and inhibition of albumin denaturation (*IAD*) are reported as IC₅₀ values. Ascorbic acid, quercetin, ibuprofen and ketoprofen were utilized as standards. Because it is a function of R_f and is determined using thin-layer chromatography, R_M is dimensionless.

The current study focused on hydrogen peroxide scavenging. Hydrogen peroxide is a kind of oxidant that is constantly produced in living tissues as a result of a variety of metabolic activities. However, detoxification is critical in order to keep it from entering hazardous reactions like the Fenton reaction [46].

Ascorbic acid and quercetin were employed as controls. They are natural substances having antioxidant characteristics that have been proven. The values we obtained varied from 59.47 µg/mL to 85.09 µg/mL for the synthesized hybrids (Table 1).

The synthesized ketoprofen analogs had modest activity when compared to ascorbic acid (24.84 $\mu\text{g}/\text{mL}$), but when compared to quercetin, hybrid **3d** had greater activity, while hybrids **3b** and **3c** had activity similar to quercetin (Figure 3).

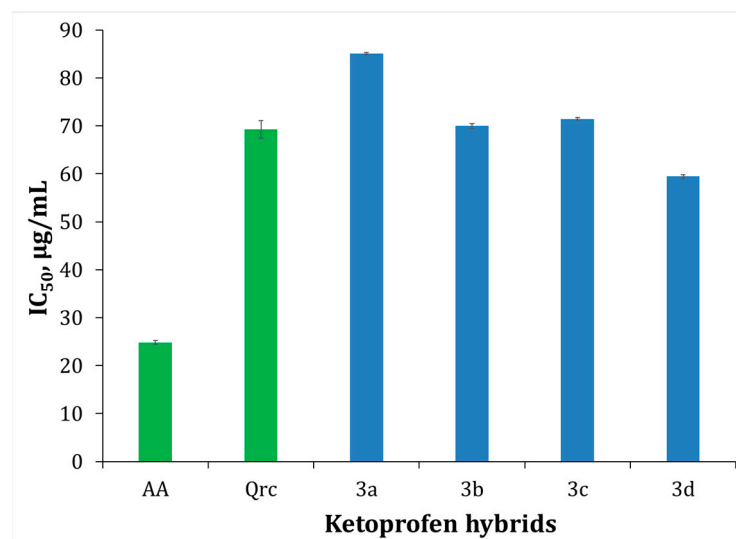


Figure 3. HPSA of the newly synthesized ketoprofen hybrid compounds. Ascorbic acid (AA) and quercetin (Qrc) were utilized as standards. HPSA results are given as IC₅₀ ($\mu\text{g}/\text{mL}$).

Despite hydrogen peroxide's low level of reactivity, it can harm cells by creating hydroxyl radicals in them [47]. The most reactive radicals are hydroxy radicals, which are considered to be responsible for some tissue damage produced by inflammation. The superoxide anion radical ($\text{O}_2^{\bullet-}$) and H_2O_2 in living organisms are converted into $\bullet\text{OH}$ and $\bullet\text{O}_2$, which cause cell damage. The inflammatory process generates a superoxide anionic radical at the site of inflammation, which is coupled with the creation of other oxidizing species, such as $\bullet\text{OH}$. It has been postulated that hydroxyl radical scavengers can function as protectors by lowering inflammation by reducing prostaglandin synthesis. As a result, removing H_2O_2 is critical in preventing the formation of $\bullet\text{OH}$.

3.3.2. Inhibition of Albumin Denaturation (IAD)

Inflammation, according to contemporary thinking, is a beneficial process that occurs as a response to a disruption or sickness. An anti-inflammatory quality of a drug or therapy is the ability to prevent inflammation or swelling. Unlike opioids, which impact the central nervous system, anti-inflammatory medicines, which account for almost half of analgesics, reduce pain by lowering inflammation. Non-steroidal anti-inflammatory drugs (NSAIDs) and steroidal anti-inflammatory drugs (SAIDs) are two types of medications frequently used to treat inflammation. NSAIDs have a number of negative side effects, particularly stomach irritation that can result in gastric ulcers [48].

The essential purpose of derivatizing ketoprofen was to eliminate the irritating and unpleasant impact of the carboxyl group. Therefore, to alter the structure of ketoprofen, we employed a variety of *N*-containing heterocyclic compounds. The novel ketoprofen hybrids were examined for IAD. The ketoprofen hybrids were compared to ibuprofen and ketoprofen, which are used to prevent inflammatory processes. The purpose of this study was to prevent albumin denaturation. This approach estimates the degree of denaturation resistance of the albumin molecule.

The study data showed that hybrids **3c** (77.18 $\mu\text{g}/\text{mL}$) and **3d** (73.59 $\mu\text{g}/\text{mL}$) possessed a higher degree of albumin protection against denaturation than the standards (Figure 4). The high activity of these compounds (**3c** and **3d**) is attributed to the presence of a 1,2,3,4-tetrahydroquinoline and 1,2,3,4-tetrahydroisoquinoline core, as well as the fact that they are less basic than **3a** and **3b**.

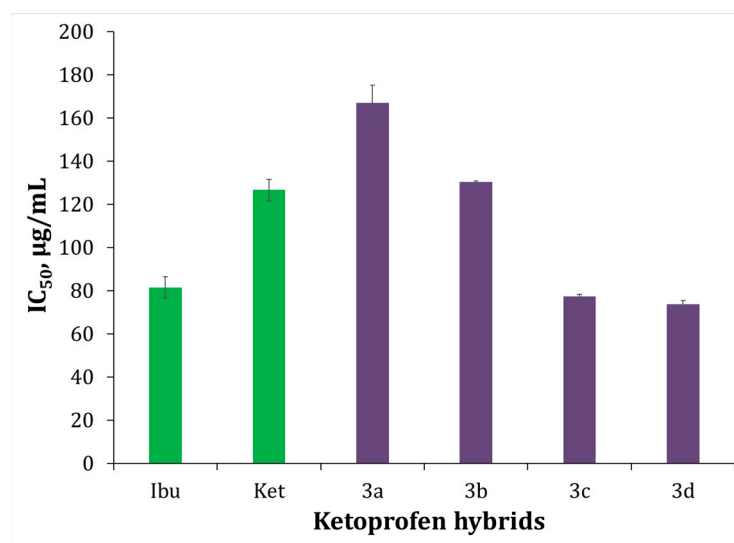


Figure 4. Inhibition of albumin denaturation (*IAD*) of newly created ketoprofen hybrid compounds. Ketoprofen (*Ket*) and ibuprofen (*Ibu*) used as benchmarks. Results for *IAD* are displayed as IC_{50} ($\mu\text{g/mL}$).

3.3.3. Experimental Determination of Lipophilicity (R_M)

Lipophilicity is a determining factor in the absorption of compounds, distribution in the body, passage through various membranes and biological barriers, metabolism, as well as excretion (these are the so-called ADME properties—absorption, distribution, metabolism, and excretion). Lipophilicity is an important factor that informs researchers to both predict and better understand the transport and importance of chemical molecules in physiological and ecological systems. It is of utmost importance for all “candidate” drugs, thanks to its extremely important role in the pharmaceutical and biotechnology industry. Lipophilicity can be measured experimentally or computed.

We used reversed-phase thin-layer chromatography to assess the lipophilicity of the resulting ketoprofen hybrids, a technique described by Hadjipavlou-Litina [49]. The results are shown in Table 1.

3.3.4. Molecular Docking

The results of the molecular docking of the enantiomers of compounds **3a–d** to the four sites of albumin given by AutoDock Vina are presented in Table 2, while the results of AutoDock are presented in Table 3.

Table 2. The results of the docking study were made using AutoDock Vina expressed as the binding affinity of the studied compounds to the four targeted sites of HSA expressed as a variation of Gibbs free energy (ΔG kcal/mol).

Compound	Isomer	Sudlow 1	Sudlow 2	Site 3	Cleft
3a	R	−8.5	−10.3	−11.5	−10.3
	S	−8.3	−10.5	−12.1	−10.0
3b	R	−8.8	−10.5	−11.7	−10.7
	S	−8.5	−11.1	−11.6	−10.2
3c	R	−10.3	−12.2	−12.9	−11.8
	S	−9.8	−12.5	−12.8	−11.2
3d	R	−10.0	−12.1	−12.4	−11.8
	S	−9.2	−12.0	−12.2	−11.6

Table 3. The results of the docking study were made using AutoDock expressed as the binding affinity of the studied compounds to the four targeted sites of HSA expressed as a variation of Gibbs free energy (ΔG kcal/mol) and the clustering analysis of the poses.

Compound	Isomer	Sudlow 1		Sudlow 2		Site 3		Cleft	
		ΔG	%C	ΔG	%C	ΔG	%C	ΔG	%C
3a	R	−8.30	20.5	−9.59	30.0	−10.80	49	−8.81	31.5
	S	−8.27	15.5	−9.74	14.5	−10.60	36	−8.79	26.5
3b	R	−8.81	16.5	−9.82	13.5	−11.47	116	−9.10	41.5
	S	−8.53	4.5	−10.16	24.0	−11.19	68	−9.12	18.5
3c	R	−9.80	18.5	−11.04	27.5	−12.65	104	−10.39	53.0
	S	−9.72	29.0	−11.41	40.5	−11.57	44	−9.95	44.5
3d	R	−9.81	7.0	−11.53	38.5	−12.80	56	−10.58	39.5
	S	−9.69	10.0	−11.44	36.0	−12.20	43	−10.46	49.0

%C: percent of conformations in the same 2Å RMSD cluster of atom coordinates.

The analysis of the results obtained after the docking of the ligands at the four albumin sites using AutoDock Vina shows a major difference in interactions, depending on the size of the heterocycle from the structure of the compounds and less influenced by the type of the isomer.

The compounds from the present series that have the highest affinity for albumin are tetrahydroquinoline derivative **3c** and tetrahydroisoquinoline derivative **3d**. Compounds **3a** and **3b** (pyrrolidine and piperidine, respectively) have, for the four studied sites, a lower affinity than compounds **3c** and **3d**.

Taking into account the affinity for the four sites, compounds exhibit the highest affinity for site 3. The affinity for the site Sudlow 2 is lower than for site 3, while the affinity for the cleft site is lower than for Sudlow 2. From the present series of compounds, they exhibit for Sudlow 1, the lowest affinity, compared to the other three sites.

The results of the docking study using AutoDock for cross-validation of the results given by AutoDock Vina share the same pattern, the affinity of the compounds for albumin being influenced by the size of the heterocycle from the structure of the compounds and less by the type of enantiomer. The most reproducible conformations of the compounds according to the RMSD of the atom coordinates are the ones for compounds **3c** and **3d**. For them, the percentage of conformations from their total conformations generated are found in the same cluster with the top binding conformation is higher than the percentage for **3a** and **3b**. Considering this observation, it can be concluded that compounds **3c** and **3d** have a more repetitive binding in the studied sites compared to compounds **3a** and **3b**, confirming this reproducibility through the repeatability of the conformations found in approximately the same area.

The depiction of the interaction between the ligands and albumin was presented for both enantiomers of a compound, chosen from the present series as the best binding pair of enantiomers on a specific site (Sudlow 2, site 3 and cleft). No depiction was made for any ligand in Sudlow 1 site because the molecular docking study performed on both software indicated that the respective site has a marginal role in the binding of the compounds from the present series.

The Sudlow 2 site, being mainly hydrophobic, comprised of Leu460, Val456, Leu457, Leu453, Leu387, Val433, Leu430 and Val426, easily fits the lipophilic moieties of compounds **3a–d**. Both enantiomers of compounds **3c** and **3d** are involved in a π - π stacking with Tyr411, while the amidic oxygen acts like a hydrogen bond acceptor from the phenol of Tyr411. The ketone of ligands can interact with the sidechain of Asn391 as a hydrogen bond acceptor and with the positively charged sidechain of Arg410 via an ion-dipole interaction.

Visual analysis of the binding poses of enantiomers of **3c** indicates that there are some differences in the binding mode of the two isomers (Figure 5), but mainly the difference between them is minor.

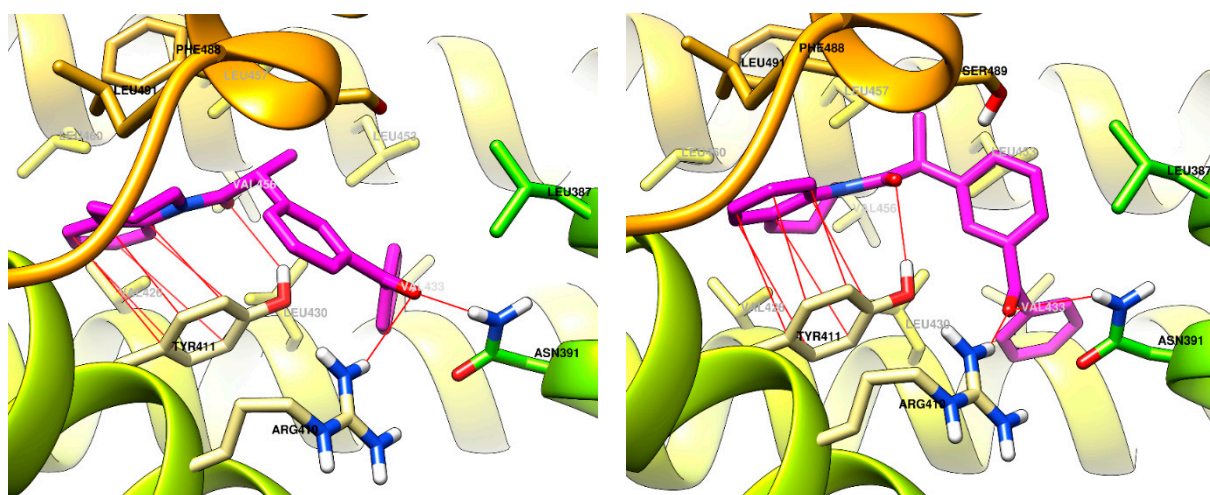


Figure 5. The best binding conformation of enantiomers of compound **3c** R (left) and S (right) in the Sudlow 2 site of albumin. Carbon atoms of **3c** are depicted in magenta.

The binding of **3d** enantiomers in site 3 of albumin is depicted in Figure 6. In both cases, the positively charged sidechain of Arg186 interacts with the benzene ring of tetrahydroisoquinoline fragment through a π -cation interaction. The pair Tyr161-Tyr138 are involved in a double π - π stacking with one of the benzenes of **3d**, for enantiomer **3dR** is expected to appear two supplementary interactions: one of the ketones with the peptide bridge Tyr138-Leu139 and a hydrogen bond between Tyr161 as a donor and the nitrogen atom of **3d** as acceptor.

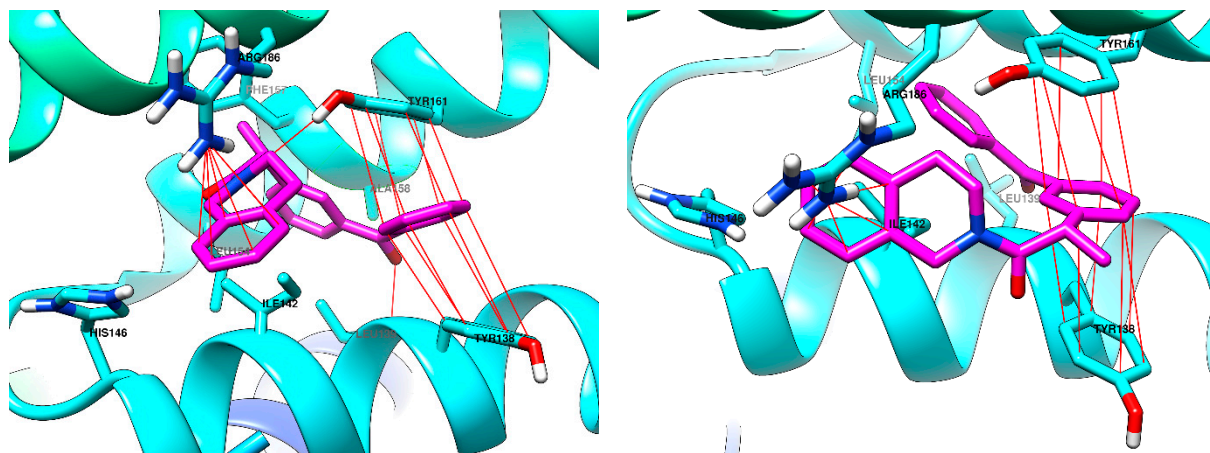


Figure 6. **3d** in site 3. The best binding conformation of enantiomers of compound **3d** R (left) and S (right) in site 3 of albumin. Carbon atoms of **3d** are depicted in magenta.

The binding of **3d** enantiomers in the cleft of albumin is depicted in Figure 7. Both enantiomers are involved with the terminal benzene ring in a π - π stacking interaction with Tyr452. The ketone of **3d** is expected to interact with the sidechain of Asn429 via a hydrogen bond as an acceptor. The amidic oxygen of **3d** is expected to interact with the positively charged sidechain of Lys190 in the case of enantiomer R, while in the case of S enantiomer is expected to interact with the amide bridge between Val455-Val456. The tetrahydroisoquinoline fragment of **3d** of both enantiomers is predicted to interact with some hydrophobic residues, such as Leu463 or Pro421.

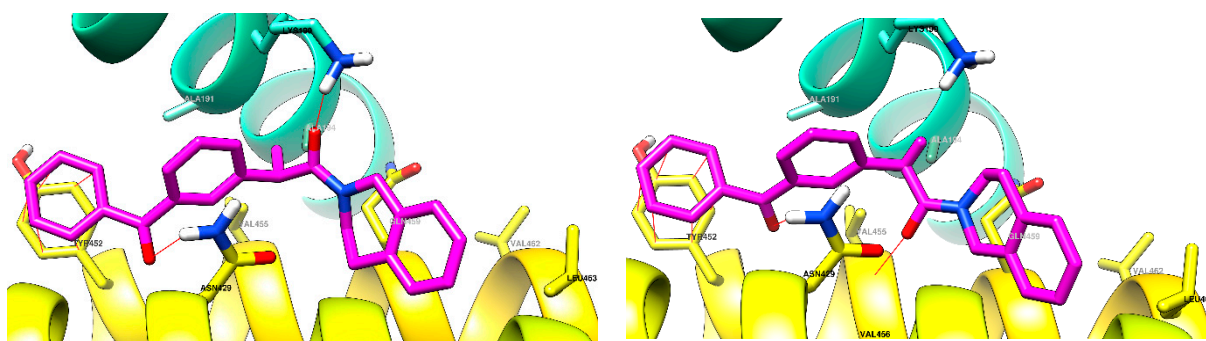


Figure 7. The best binding conformation of enantiomers of compound **3d** **R** (left) and **S** (right) in the cleft site of albumin. Carbon atoms of **3d** are depicted in magenta.

3.3.5. Molecular Dynamics

The stability of the albumin complexes with the best binding ligands in the molecular docking study performed with AutoDock vina with the variation of the Gibbs free energy in the first half of energies was evaluated during 100 ns of molecular dynamics simulation. According to the results of the molecular docking study, all the potential complexes of the studied compounds in site 3 of albumin were simulated, and the complexes of compounds **3c** and **3d** in the site Sudlow 2 and in the cleft site. None of the complexes were simulated with ligands docked into the Sudlow 1 site due to their low affinity to the respective site.

The stability of the protein–ligand simulated systems in the molecular dynamics study was expressed by calculating the average root-mean-square deviation (RMSD) of the backbone of the protein, the average root-mean-square deviation (RMSD) of the heavy atoms of ligands, the radius of gyration (RG) of the protein and the hydrogen bonds between the ligand and the protein.

An overview of the results of the molecular dynamics study is presented in Table 4 as the RMSD of the backbone of the protein, in Table 5 as the RMSD of the heavy atoms of ligands, Table 6 as RG of the protein, and in Table 7 the evolution of the hydrogen bonds between protein and ligands.

Table 4. The root mean square deviation of the backbone of the protein from the systems evaluated in the molecular dynamics study (nm).

System Evaluated	Sudlow 1	Sudlow 2	Site 3	Cleft
apo + 3a[R]	-	-	0.33	-
apo + 3a[S]	-	-	0.28	-
apo + 3b[R]	-	-	0.30	-
apo + 3b[S]	-	-	0.41	-
apo + 3c[R]	-	0.36	0.25	0.23
apo + 3c[S]	-	0.29	0.30	0.36
apo + 3d[R]	-	0.24	0.36	0.26
apo + 3d[S]	-	0.24	0.34	0.38
apo		0.38		

- not tested.

Table 5. The root mean square deviation of the heavy atoms of the ligands from the systems evaluated in the molecular dynamics study (nm).

System Evaluated	Sudlow 1	Sudlow 2	Site 3	Cleft
apo + 3a[R]	-	-	0.35	-
apo + 3a[S]	-	-	0.26	-
apo + 3b[R]	-	-	0.27	-

Table 5. *Cont.*

System Evaluated	Sudlow 1	Sudlow 2	Site 3	Cleft
apo + 3b[S]	-	-	1.34	-
apo + 3c[R]	-	0.24	0.32	0.41
apo + 3c[S]	-	0.25	0.23	0.20
apo + 3d[R]	-	0.47	0.59	0.27
apo + 3d[S]	-	0.26	0.62	0.36

- not tested.

Table 6. The radius of gyration of the protein from the systems evaluated in the molecular dynamics study (nm).

System Evaluated	Sudlow 1	Sudlow 2	Site 3	Cleft
apo + 3a[R]	-	-	2.85	-
apo + 3a[S]	-	-	2.78	-
apo + 3b[R]	-	-	2.84	-
apo + 3b[S]	-	-	2.89	-
apo + 3c[R]	-	2.75	2.78	2.77
apo + 3c[S]	-	2.80	2.82	2.77
apo + 3d[R]	-	2.79	2.80	2.81
apo + 3d[S]	-	2.79	2.77	2.78
apo		2.78		

- not tested.

Table 7. The average number of hydrogen bonds between the ligand and the protein in the systems evaluated in the molecular dynamics study (no/ns).

System Evaluated	Sudlow 1	Sudlow 2	Site 3	Cleft
apo + 3a[R]	-	-	0.01	-
apo + 3a[S]	-	-	0.12	-
apo + 3b[R]	-	-	0.12	-
apo + 3b[S]	-	-	0.21	-
apo + 3c[R]	-	0.17	0.46	0.05
apo + 3c[S]	-	0.02	0.19	0.02
apo + 3d[R]	-	0.00	0.06	0.02
apo + 3d[S]	-	0.33	0.37	0.03

- not tested.

It can be seen that compounds **3a** and **3b** (pyrrolidine and piperidine derivatives) gives complexes with albumin, which are less stable than those of compounds **3c** and **3d** (tetrahydroquinoline and tetrahydroisoquinoline hybrids). The increase of the nitrogen ring with a supplementary benzene ring leads to better stabilization of the albumin. On average, taking into account the data available for the complexes resulting from the binding of ligands into site 3, RMSD of the backbone of the protein is higher for complexes with compounds **3a** and **3b** than those with **3c** and **3d** (0.33 nm vs. 0.31 nm). The same trend is identified for the average RMSD of the ligands (0.56 nm vs. 0.44 nm) and the average RG of the protein (0.56 nm vs 0.44 nm). The highest stabilization of the backbone of the protein, expressed as the lowest RMSD of the backbone, was identified as **3cR** into site 3 and cleft, **3dR** into Sudlow 2 and cleft and **3dS** in Sudlow 2.

The changes in the position of the ligand expressed as RMSD of the heavy atoms of the ligand indicate that most of the predicted complexes are stable. Some exceptions were identified, such as compound **3bS** in site 3, **3cR** in cleft, **3dR** in Sudlow 2 and site 3 and **3dS** in site 3, which move significantly from their initial position.

Evaluating the hydrogen bonding between the ligand and the protein **3cR** and **3dS** are the ones that interact more via this type of bond than the other compounds.

Overall, the resumed data indicates that there is no obvious connection between the type of enantiomer of each compound and the parameters evaluated for the resulting complexes to express their stability. The stability of the complexes is influenced simultaneously by the type of nitrogen ring and the type of enantiomer.

Detailed information regarding the evolution of the stability of the complexes of compounds **3c** and **3d** in the Sudlow site 2 are presented in Table S1, of all **3a–d** compounds in site 3 of albumin in tables Tables S2–S4 for compounds **3c** and **3d** in the cleft site of albumin.

The data obtained after simulation of the complexes of compounds **3c** and **3d** into the Sudlow 2 site indicates that both compounds gave complexes with albumin with similar RMSD to the apo form of the protein. The complexes of **3d** (both enantiomers) lead to the best stabilization of the protein in terms of the RMSD of the protein backbone. Into the specified site, **3cR**, **3cS** and **3dS** have the lowest movement, compared to **3dR**, which has a significant change in position during the simulation.

3cR and **3dS** are supposed to have significantly more hydrogen bonds compared to the other enantiomer. Again, this observation confirms the previous observation that the interaction between each enantiomer and protein is influenced by the type of nitrogen ring and the type of enantiomer.

When docked into site 3 of albumin, compounds **3aS** and **3cR** gave the most stable complexes in the present series. Significant instability of the complexes given by the other compounds was identified as follows: **3bS** leaves site 3 after approximately 20 ns, and **3cR** suffers a significant change of position at approximately 35 ns, resulting in continuous changes in the coordinates of the atoms of the backbone of albumin, **3cS** gave a stable complex until 85 ns of simulation, while both enantiomers of **3d** won't reach a convergence, having a continuous movement into the site 3 of albumin.

The complex of **3dR** in site 3 of albumin is the most stable from the current series. A high degree of stability expressed in terms of RMSD of the protein backbone was identified too, but it didn't reach a convergence point during the simulation and the RMSD of the protein backbone was found to slowly and continuously increase until the simulation ended. Anyhow, both R enantiomers gave more stable complexes than S enantiomers when docked into the cleft of albumin. **3cS** moved less into the cleft than **3cR**, but the RMSD of the backbone was similar to the apo form and even decreased during simulation, compared to **3cS**. **3dS** exhibited a significant change in position at approximately 70 ns, affecting a little the RMSD of the backbone of the protein at that time, increasing the RMSD of the protein backbone from complex over the apo form.

4. Conclusions

In conclusion, we have obtained four novel hybrid compounds combining a ketoprofen skeleton and an *N*-containing hetero ring. The newly discovered molecules have been thoroughly characterized and were subjected to a comprehensive mass spectral analysis. According to the *in vitro* and *in silico* experiments, the hybrid compounds have considerable *HPSA* and *in vitro* anti-inflammatory action as measured by *IAD*. Despite their lipophilic character, compounds **3b–d** have *HPSA* values comparable to quercetin. To neutralize damaging radicals in the cell membrane, lipophilic antioxidants are required. *In vitro*, anti-inflammatory activity was evaluated by *IAD*, as well as by molecular docking and molecular dynamics. Ligand–albumin interactions were demonstrated for both enantiomers of compound **3a–d**, which were chosen from the current series as the best binding pair of enantiomers at a given site (Sudlow 2, site 3, and Cleft). The highest *in vitro* anti-inflammatory efficacy is shown by hybrids **3c** and **3d**, which stabilize the albumin macromolecule by forming ligand–albumin complexes with Sudlow 2, site 3, and cleft. This interaction is responsible for preventing albumin denaturation during inflammatory processes. The stability of the albumin macromolecule is due to the fact that hybrids **3c** and **3d** participate in π - π arrangement with Tyr411 (Sudlow 2), with the pair Tyr161-Tyr138 (site 3), and Tyr452 (cleft). Furthermore, H-bonds are generated with the amide, ketone,

and oxygen with the polar amino acid residues implicated in the Sudlow 2, site 3, and cleft structures. The in-silico studies completely confirm our *in vitro* experimental results for anti-inflammatory effects. All of this demonstrates that the hybrid compounds we synthesized inherit ketoprofen's anti-inflammatory capabilities, making them excellent candidates for future medications.

Supplementary Materials: The following supporting information can be downloaded at: <https://www.mdpi.com/article/10.3390/pr11061837/s1>, Figure S1: ¹H-NMR spectrum of compound **3a**; Figure S2: ¹H-NMR spectrum of compound **3b**; Figure S3: ¹H-NMR spectrum of compound **3c**; Figure S4: ¹H-NMR spectrum of compound **3d**; Figure S5: ¹³C-NMR spectrum of compound **3a**; Figure S6: ¹³C-NMR spectrum of compound **3b**; Figure S7: ¹³C-NMR spectrum of compound **3c**; Figure S8: ¹³C-NMR spectrum of compound **3d**; Figure S9: UV spectrum of compound **3a**; Figure S10: UV spectrum of compound **3b**; Figure S11: UV spectrum of compound **3c**; Figure S12: UV spectrum of compound **3d**; Figure S13: ESI-HRMS of compound **3a**; Figure S14: Mass spectrum of **3a** obtained by positive ion ESI-MS/MS; Figure S15: ESI-HRMS of compound **3b**; Figure S16: Mass spectrum of **3b** obtained by positive ion ESI-MS/MS; Figure S17: ESI-HRMS of compound **3c**; Figure S18: Mass spectrum of **3c** obtained by positive ion ESI-MS/MS; Figure S19: ESI-HRMS of compound **3d**; Figure S20: Mass spectrum of **3d** obtained by positive ion ESI-MS/MS; Table S1: RMSD of protein backbone, RMSD of ligands and RG of protein in the molecular dynamics study when ligands **3c** and **3d** were docked into the Sudlow 2 site; Table S2: RMSD of protein backbone, RMSD of ligands and RG of protein in the molecular dynamics study when ligands **3a** and **3b** were docked into the site 3 of albumin; Table S3: RMSD of protein backbone, RMSD of ligands and RG of protein in the molecular dynamics study when ligands **3c** and **3d** were docked into the site 3 of albumin; Table S4: RMSD of protein backbone, RMSD of ligands and RG of protein in the molecular dynamics study when ligands **3c** and **3d** were docked into the cleft of albumin.

Author Contributions: Conceptualization, S.M. and D.B.; methodology, I.I.; software, G.M., S.M., S.O. and O.O.; validation, S.M., I.I. and D.B.; formal analysis, N.B., S.M., G.M., D.B., S.O. and P.N.; investigation, I.I.; resources, I.I. and O.O.; data curation, S.M.; writing—original draft preparation, S.M., D.B. and G.M.; writing—review and editing, S.M. and D.B.; visualization, G.M.; supervision, I.I., S.O. and O.O.; project administration, S.M.; funding acquisition, I.I. and O.O. All authors have read and agreed to the published version of the manuscript.

Funding: This research was funded by the Scientific Research Fund of the University of Plovdiv, grant number ФП23-ХФ-005.

Data Availability Statement: The data presented in this study are available in this article and supporting Supplementary Materials.

Conflicts of Interest: The authors declare no conflict of interest.

References

1. Qui, M.; Fu, X.; Fu, P.; Huang, J. Construction of aziridine, azetidine, indole and quinolone-like heterocycles via Pd-mediated C-H activation/annulation strategies. *Org. Biomol. Chem.* **2022**, *20*, 1339–1359. [[CrossRef](#)]
2. Kumar, P.; Satbhaiya, S. Chapter 6—proline and proline-derived organocatalysts in the synthesis of heterocycles. In *Green Synthetic Approaches for Biologically Relevant Heterocycles. Volume 2: Green Catalytic Systems and Solvents Advances in Green and Sustainable Chemistry*, 2nd ed.; Elsevier: Amsterdam, The Netherlands, 2021; pp. 215–251. [[CrossRef](#)]
3. Carroll, I. Epibatidine analogs synthesized for characterization of nicotinic pharmacophores—A review. *Heterocycles* **2009**, *79*, 99–120. [[CrossRef](#)]
4. Amarouche, L.; Mehdid, M.; Brahimi, F.; Belkhadem, F.; Karmaoui, M.; Othman, A. Synthesis of some 2-substituted pyrrolidine alkaloid analogues: N-benzyl-2-(5-substituted 1,3,4-oxadiazolyl) pyrrolidine derivatives and pharmacological screening. *J. Saudi Chem. Soc.* **2022**, *26*, 101448. [[CrossRef](#)]
5. Singh, L.; Upadhyay, A.; Dixit, P.; Singh, A.; Yadav, D.; Chhavi, A.; Konar, S.; Srivastava, R.; Pandey, S.; Devkota, H.; et al. A Review of chemistry and pharmacology of piperidine alkaloids of pinus and related genera. *Curr. Pharm. Biotechnol.* **2022**, *23*, 1132–1141. [[CrossRef](#)]
6. Vitaku, E.; Smith, D.; Njardarson, J. Analysis of the structural diversity, substitution patterns, and frequency of nitrogen heterocycles among U.S. FDA approved pharmaceuticals. *J. Med. Chem.* **2014**, *57*, 10257–10274. [[CrossRef](#)] [[PubMed](#)]
7. Srinivasan, K. Black pepper and its pungent principle-piperine: A review of diverse physiological effects. *Crit. Rev. Food Sci. Nutr.* **2007**, *47*, 735–748. [[CrossRef](#)] [[PubMed](#)]

8. Sridharan, V.; Suryavanshi, P.; Menéndez, C. Advances in the chemistry of tetrahydroquinolines. *Chem. Rev.* **2011**, *111*, 7157–7259. [CrossRef]
9. Swidorski, J.; Liu, Z.; Yin, Z.; Wang, T.; Carini, D.; Rahematpura, S.; Zheng, M.; Johnson, K.; Zhang, S.; Lin, P.; et al. Inhibitors of HIV-1 attachment: The discovery and structure-activity relationships of tetrahydroisoquinolines as replacements for the piperazine benzamide in the 3-glyoxylyl 6-azaindole pharmacophore. *Bioorg. Med. Chem. Lett.* **2016**, *26*, 160–167. [CrossRef]
10. Liu, X.-H.; Zhu, J.; Zhou, A.; Song, B.-A.; Zhu, H.-L.; Bai, L.-S.; Bhadury, P.; Pan, C.-X. Synthesis, structure and antibacterial activity of new 2-(1-(2-(substituted-phenyl)-5-methyloxazol-4-yl)-3-(2-substituted-phenyl)-4,5-dihydro-1H-pyrazol-5-yl)-7-substituted-1,2,3,4-tetrahydroisoquinoline derivatives. *Bioorg. Med. Chem.* **2009**, *17*, 1207–1213. [CrossRef]
11. Kumar, A.; Katiyar, S.; Gupta, S.; Chauhan, P. Synthesis of new substituted triazino tetrahydroisoquinolines and β -carbolines as novel antileishmanial agents. *Eur. J. Med. Chem.* **2006**, *41*, 106–113. [CrossRef] [PubMed]
12. Zhu, J.; Lu, J.; Zhou, Y.; Li, Y.; Cheng, J.; Zheng, C. Design, synthesis, and antifungal activities *in vitro* of novel tetrahydroisoquinoline compounds based on the structure of lanosterol 14 α -demethylase (CYP51) of fungi. *Bioorg. Med. Chem. Lett.* **2006**, *16*, 5285–5289. [CrossRef]
13. Tiwari, R.; Singh, D.; Singh, J.; Chhillar, A.; Chandra, R.; Verma, A. Synthesis, antibacterial activity and QSAR studies of 1,2-disubstituted-6,7-dimethoxy-1,2,3,4-tetrahydroisoquinolines. *Eur. J. Med. Chem.* **2006**, *41*, 40–49. [CrossRef]
14. Faheem, R.; Kumar, B.; Sekhar, K.; Chander, S.; Kunjiappan, S.; Murugesan, S. Medicinal chemistry perspectives of 1,2,3,4-tetrahydroisoquinoline analogs—Biological activities and SAR studies. *RSC Adv.* **2021**, *11*, 12254–12287. [CrossRef] [PubMed]
15. Fischer, J.; Robin, G.C. *Analogue-Based Drug Discovery*; John Wiley & Sons: Hoboken, NJ, USA, 2006; p. 520. ISBN 9783527607495.
16. Jachak, S. Cyclooxygenase inhibitory natural products: Current status. *Curr. Med. Chem.* **2006**, *13*, 659–678. [CrossRef] [PubMed]
17. Manolov, S.; Ivanov, I.; Bojilov, D. Synthesis of New 1,2,3,4-Tetrahydroquinoline Hybrid of Ibuprofen and Its Biological Evaluation. *Molbank* **2022**, *2022*, M1350. [CrossRef]
18. Manolov, S.; Ivanov, I.; Bojilov, D. Microwave-assisted synthesis of 1,2,3,4-tetrahydroisoquinoline sulfonamide derivatives and their biological evaluation. *J. Serb. Chem. Soc.* **2021**, *86*, 139–151. [CrossRef]
19. Trott, O.; Olson, A. AutoDock Vina: Improving the speed and accuracy of docking with a new scoring function, efficient optimization, and multithreading. *J. Comput. Chem.* **2009**, *31*, 455–461. [CrossRef]
20. Morris, G.; Huey, R.; Lindstrom, W.; Sanner, M.; Belew, R.; Goodsell, D.; Olson, A. AutoDock4 and AutoDockTools4: Automated Docking with Selective Receptor Flexibility. *J. Comput. Chem.* **2009**, *30*, 2785–2791. [CrossRef]
21. Berman, H.M.; Westbrook, J.; Feng, Z.; Gilliland, G.; Bhat, T.N.; Weissig, H.; Shindyalov, I.N.; Bourne, P.E. The Protein Data Bank. *Nucleic Acids Res.* **2000**, *28*, 235–242. [CrossRef]
22. Makeneni, S.; Thieker, D.F.; Woods, R.J. Applying Pose Clustering and MD Simulations To Eliminate False Positives in Molecular Docking. *J. Chem. Inf. Model.* **2018**, *58*, 605–614. [CrossRef]
23. Hanwell, M.D.; Curtis, D.E.; Lonie, D.C.; Vandermeersch, T.; Zurek, E.; Hutchison, G.R. Avogadro: An advanced semantic chemical editor, visualization, and analysis platform. *J. Cheminform.* **2012**, *4*, 17. [CrossRef]
24. Stoica, C.I.; Marc, G.; Pîrnău, A.; Vlase, L.; Aranciu, C.; Oniga, S.; Palage, M.; Oniga, O. Thiazolyl-oxadiazole derivatives targeting lanosterol 14 α -demethylase as potential antifungal agents: Design, synthesis and molecular docking studies. *Farmacia* **2016**, *64*, 390–397. Available online: https://farmaciajournal.com/wp-content/uploads/2016-03-art-11-Stoica_Cristina_Oniga_390-397.pdf (accessed on 18 March 2023).
25. Borlan, R.; Stoia, D.; Gaina, L.; Campu, A.; Marc, G.; Perde-Schrepler, M.; Silion, M.; Maniu, D.; Focsan, M.; Astilean, S. Fluorescent Phthalocyanine-Encapsulated Bovine Serum Albumin Nanoparticles: Their Deployment as Therapeutic Agents in the NIR Region. *Molecules* **2021**, *26*, 4679. [CrossRef] [PubMed]
26. Ascoli, G.; Domenici, E.; Bertucci, C. Drug binding to human serum albumin: Abridged review of results obtained with high-performance liquid chromatography and circular dichroism. *Chirality* **2006**, *18*, 667–679. [CrossRef] [PubMed]
27. Yang, F.; Zhang, Y.; Liang, H. Interactive Association of Drugs Binding to Human Serum Albumin. *Int. J. Mol. Sci.* **2014**, *15*, 3580–3595. [CrossRef]
28. Nishi, K.; Yamasaki, K.; Otagiri, M. Serum Albumin, Lipid and Drug Binding. *Subcell Biochem.* **2020**, *94*, 383–397. [CrossRef]
29. Czub, M.; Stewart, A.; Shabalin, I.; Minor, W. Organism-specific differences in the binding of ketoprofen to serum albumin. *IUCr* **2022**, *9*, 551–561. [CrossRef]
30. Zsila, F. Subdomain IB Is the Third Major Drug Binding Region of Human Serum Albumin: Toward the Three-Sites Model. *Mol. Pharm.* **2013**, *10*, 1668–1682. [CrossRef]
31. Mishra, V.; Heath, R. Structural and Biochemical Features of Human Serum Albumin Essential for Eukaryotic Cell Culture. *Int. J. Mol. Sci.* **2021**, *22*, 8411. [CrossRef]
32. Pettersen, E.; Goddard, T.; Huang, C.; Couch, G.; Greenblatt, D.; Meng, E.; Ferrin, T. UCSF Chimera—A visualization system for exploratory research and analysis. *J. Comput. Chem.* **2004**, *25*, 1605–1612. [CrossRef]
33. Abraham, M.J.; Murtola, T.; Schulz, R.; Páll, S.; Smith, J.C.; Hess, B.; Lindahl, E. GROMACS: High performance molecular simulations through multi-level parallelism from laptops to supercomputers. *SoftwareX* **2015**, *1–2*, 19–25. [CrossRef]
34. Vanommeslaeghe, K.; Hatcher, E.; Acharya, C.; Kundu, S.; Zhong, S.; Shim, J.; Darian, E.; Guvench, O.; Lopes, P.; Vorobyov, I.; et al. CHARMM general force field: A force field for drug-like molecules compatible with the CHARMM all-atom additive biological force fields. *J. Comput. Chem.* **2010**, *31*, 671–690. [CrossRef]

35. Jorgensen, W.; Chandrasekhar, J.; Madura, J.; Impey, R.; Klein, M. Comparison of simple potential functions for simulating liquid water. *J. Chem. Phys.* **1983**, *79*, 926–935. [[CrossRef](#)]
36. Lv, Z.; Wang, H.; Niu, X. Molecular dynamics simulations reveal insight into key structural elements of aaptamines as sortase inhibitors with free energy calculations. *Chem. Phys. Lett.* **2013**, *585*, 171–177. [[CrossRef](#)]
37. Jin, H.; Zhou, Z.; Wang, D.; Guan, S.; Han, W. Molecular Dynamics Simulations of Acylpeptide Hydrolase Bound to Chlorpyrifos-methyl Oxon and Dichlorvos. *Int. J. Mol. Sci.* **2015**, *16*, 6217–6234. [[CrossRef](#)]
38. Crişan, O.; Marc, G.; Nastasă, C.; Oniga, S.; Vlase, L.; Pîrnău, A.; Oniga, O. Synthesis and *in silico* approaches of new symmetric bis-thiazolidine-2,4-diones as Ras and Raf oncoproteins inhibitors. *Farmacia* **2023**, *71*, 254–263. Available online: https://farmaciajournal.com/wp-content/uploads/art-04-Crisan_Marc_Oniga_254-263.pdf (accessed on 22 March 2023).
39. Humphrey, W.; Dalke, A.; Schulten, K. VMD: Visual molecular dynamics. *J. Mol. Graph.* **1996**, *14*, 33–38. [[CrossRef](#)] [[PubMed](#)]
40. Ning, X.-Q.; Lou, S.-J.; Mao, Y.-J.; Xu, Z.-Y.; Xu, D.-Q. Nitrate-promoted selective C-H Fluorination of benzamides and benzenacetamides. *Org. Lett.* **2018**, *20*, 2445–2448. [[CrossRef](#)]
41. Uludağ, M.; Ergün, B.; Alkan, D.; Ercan, N.; Özkan, G.; Banoğlu, E. Stable ester and amide conjugates of some NSAIDs as analgesic and antiinflammatory compounds with improved biological activity. *Turk. J. Chem.* **2011**, *35*, 427–439. [[CrossRef](#)]
42. Manolov, S.; Ivanov, I.; Bojilov, D.; Nedialkov, P. Synthesis, *In Vitro* Anti-Inflammatory Activity, and HRMS Analysis of New Amphetamine Derivatives. *Molecules* **2023**, *28*, 151. [[CrossRef](#)]
43. Manolov, S.; Ivanov, I.; Bojilov, D.; Nedialkov, P. Synthesis, *in silico*, and *in vitro* biological evaluation of new furan hybrid molecules. *Processes* **2022**, *10*, 1997. [[CrossRef](#)]
44. Galano, A.; Macías-Ruvalcaba, N.; Campos, O.; Pedraza-Chaverri, J. Mechanism of the OH radical scavenging activity of nordihydroguaiaretic acid: A combined theoretical and experimental study. *J. Phys. Chem. B* **2010**, *114*, 6625–6635. [[CrossRef](#)]
45. Halliwell, B.; Gutteridge, J. *Free Radicals in Biology and Medicine*; Clarendon Press: Oxford, UK, 1985; p. 346.
46. Mansouri, A.; Makris, D.; Kefalas, P. Determination of hydrogen peroxide scavenging activity of cinnamic and benzoic acids employing a highly sensitive peroxyoxalate chemiluminescence-based assay: Structure-activity relationships. *J. Pharm. Biomed. Anal.* **2005**, *39*, 22–26. [[CrossRef](#)]
47. Ebrahimzadeh, M.; Nabavi, S.; Nabavi, S.; Bahramian, F.; Bekhradnia, A. Antioxidant and free radical scavenging activity of *H. officinalis* L. var. *angustifolius*, *V. odorata*, *B. hircana* and *C. speciosum*. *Pak. J. Pharm. Sci.* **2010**, *23*, 29–34.
48. Jayashree, V.; Bagyalakshmi, S.; Manjula Devi, K.; Richard Daniel, D. *In vitro* anti-inflammatory activity of 4-benzylpiperidine. *Asian J. Pharm. Clin. Res.* **2016**, *9*, 108–110. [[CrossRef](#)]
49. Pontiki, E.; Hadjipavlou-Litina, D. Synthesis and pharmacological evaluation of novel aryl-acetic acid inhibitors of lipoygenase, antioxidants, and anti-inflammatory agents. *Bioorg. Med. Chem.* **2007**, *15*, 5819–5827. [[CrossRef](#)] [[PubMed](#)]

Disclaimer/Publisher’s Note: The statements, opinions and data contained in all publications are solely those of the individual author(s) and contributor(s) and not of MDPI and/or the editor(s). MDPI and/or the editor(s) disclaim responsibility for any injury to people or property resulting from any ideas, methods, instructions or products referred to in the content.